

DTIC FILE COPY

①

AD-A179 390



DTIC
ELECTE
APR 17 1987
S
D
D

FREQUENCY SHIFT MEASUREMENTS
OF THE Q(1) AND Q(2) LINES OF H₂
USING HIGH RESOLUTION CW
COHERENT ANTI-STOKES RAMAN SPECTROSCOPY

THESIS

Mark P. Jelonek
Second Lieutenant
USAF
AFIT/GEP/ENP/86D-5

DISTRIBUTION STATEMENT A
Approved for public release;
Distribution Unlimited

DEPARTMENT OF THE AIR FORCE
AIR UNIVERSITY
AIR FORCE INSTITUTE OF TECHNOLOGY

Wright-Patterson Air Force Base, Ohio

87 4 16 041

AFIT/GEP/ENP/86

DTIC
ELECTE
APR 17 1987
S D D

FREQUENCY SHIFT MEASUREMENTS
OF THE Q(1) AND Q(2) LINES OF H₂
USING HIGH RESOLUTION CW
COHERENT ANTI-STOKES RAMAN SPECTROSCOPY

THESIS

Mark P. Jelonek
Second Lieutenant
USAF
AFIT/GEP/ENP/86D-5

Approved for public release; distribution unlimited

AFIT/GEP/ENP/86D-5

FREQUENCY SHIFT MEASUREMENTS
OF THE Q(1) AND Q(2) LINES OF H₂
USING HIGH RESOLUTION CW
COHERENT ANTI-STOKES RAMAN SPECTROSCOPY
THESIS

Presented to the Faculty of the School of Engineering
of the Air Force Institute of Technology
Air University
In Partial Fulfillment of the
Requirements for the Degree of
Master of Science in Engineering Physics

Mark P. Jelonek, B.S.
Second Lieutenant, USAF

December 1986



Accession For	
NTIS CRA&I	<input checked="" type="checkbox"/>
DTIC TAB	<input type="checkbox"/>
Unannounced	<input type="checkbox"/>
Justification	
By	
Distribution/	
Availability Codes	
Dist	Avail and/or Special
A-1	

Approved for public release; distribution unlimited

Acknowledgements

A master's thesis is principally a learning experience, and I feel that my project completely fulfilled that expectation. Not only did I acquire hands-on experience in a multiplicity of experimental disciplines, but I also received my "baptism under fire" of the pitfalls, road blocks, equipment failures, and out-and-out aggravation that is supposed to accompany experimental research. I would not, however, trade the tremendous amount of knowledge of theory, experiment, and improvisation that I swallowed in these last few months for anything in the world.

I owe a deep debt to many people without whom I could never have completed my project. There are no words to describe my gratitude to my advisor, Dr. Won B. Roh, for the time and energy he devoted exclusively to helping me. I would also like to thank all the members of the class of GEP-86D. Each helped me in his own way whether it was in the lab proper or just with a word of encouragement. Finally, I would like to thank John Brohas at the AFIT shop and the Physics Department laboratory staff, Rick Patton, Walt Pemberton, and Bill Evans, for their support and for putting up with my seemingly incessant requests. To all of you, thank you.

Mark P. Jelonek

Table of Contents

	Page
Acknowledgements	ii
List of Figures	iv
List of Tables	v
List of Symbols	vi
Abstract	viii
I. Introduction	1
II. Theory	4
Generation of CARS Photons	4
Third-order CARS Susceptibility	6
Frequency Shift	10
III. Frequency Stabilization of the Argon-ion Laser	12
Laser Frequency Drift	12
Phase Sensitive Detection	14
Servo Control System	16
IV. Experimental Procedure	20
Experimental Apparatus	20
Data Collection	25
V. Data and Analysis	27
Data	27
Analysis	33
VI. Conclusions and Recommendations	41
Bibliography	43
Vita	44

List of Figures

Figure	Page
1. Generation of anti-Stokes photons	5
2. Dispersion curve produced by tuning the Fourier frequency spectrum of a frequency modulated signal across a Fabry-Perot transmission peak	15
3. Schematic diagram of frequency stabilization system	17
4. Schematic diagram of experimental apparatus .	21
5. Sample scan of Q(1) transition at 10 atmospheres	28
6. Sample scan of Q(2) transition at 5 atmospheres	29
7. Relative frequency shift, pressure broadened linewidth, and signal intensity of the Q(2) transition at 5 and 15 atmospheres . . .	34
8. Q(1) frequency shift as a function of pressure .	35
9. Q(2) frequency shift as a function of pressure .	36

List of Tables

Table		Page
I.	Stokes frequencies of the Q(1) transition .	31
II.	Stokes frequencies of the Q(2) transition .	32
III.	Comparison of the frequency shift coefficients for the Q(1) transition	37
IV.	Comparison of the frequency shift coefficients for the Q(2) transition	38

List of Symbols

A_p, A_s, A_s^*	Electric field amplitudes for the pump, Stokes, and the Stokes complex conjugate
a_j	Linear frequency shift coefficient
b_j	Quadratic frequency shift coefficient
c	Speed of light
c.c.	Complex conjugate
F	Force
\mathcal{H}_I	Interaction Hamiltonian
I	Signal irradiance
k_p, k_s	Pump and Stokes wave number frequencies
L	Cavity length
N	Molecular number density
n	Index of refraction
$\vec{P}, \vec{P}^L, \vec{P}^{NL}, P_{\text{CARS}}$	Polarization vector, linear, nonlinear, and CARS polarizations
p	Pressure
ζ	Molecular displacement amplitude
$\nu_{Q(J)}$	Stokes frequency of a Q-branch transition
q	Integer; internuclear displacement
\bar{R}	Mean molecular separation
\bar{v}	Mean molecular velocity

List of Symbols (continued)

α	Polarizability; coefficient of linear expansion
β	Modulation index
Γ	Damping constant; fullwidth at half maximum
Δ	Differential change
ϵ_0	Permittivity of free space
ν	Laser frequency in Hertz
ρ	Gas density in amagats
σ_b, σ_s	Real and imaginary optical cross sections
χ	Medium susceptibility
Ω	Optical carrier frequency
ω	Modulation frequency
$\Delta\omega$	Frequency shift
$\omega_{AS}, \omega_p, \omega_s$	Anti-Stokes, pump, and Stokes angular frequencies

Abstract

Linear and quadratic frequency shift coefficients were determined for the Q(1) and Q(2) lines of H_2 using cw coherent anti-Stokes Raman spectroscopy (CARS). The linear coefficients were accurate to three significant digits which is an order of magnitude better than any previous work, and the quadratic coefficients determined were of comparable accuracy to those of other published results. Significant improvements were made in an existing CARS apparatus including active frequency stabilization of the Ar-ion laser and the incorporation of multiple Pellin-Broca prisms to reduce background noise. The frequency stabilization of the Ar-ion and ring-dye lasers allowed extremely accurate measurements of the frequency shifts of the anti-Stokes line on the basis of Stokes frequency measurement over a range of pressures from 2 to 40 atmospheres. A Fabry-Perot interferometer provided a relative frequency marker for the determination of the line shift along with I_2 absorption peaks which provided an absolute frequency reference. The coefficients were compared to those determined by other researchers using different methods. The high accuracy of the measurements added further credence to the effectiveness of cw CARS as a high resolution spectroscopic tool.

FREQUENCY SHIFT MEASUREMENTS
OF THE Q(1) AND Q(2) LINE OF H₂
USING HIGH RESOLUTION CW
COHERENT ANTI-STOKES RAMAN SPECTROSCOPY

I. Introduction

This thesis describes the theory, experiment, and results of frequency shift measurements of the Q(1) and Q(2) lines of H₂ using high resolution cw coherent anti-Stokes Raman spectroscopy (CARS). The following is a brief overview of the CARS process, the uses of CARS as a diagnostic tool, and its relevance to the Air Force along with the interest in frequency shift measurements.

Coherent anti-Stokes Raman scattering is a third-order nonlinear optical mixing process which occurs when two high powered lasers are focussed simultaneously in a medium. The interaction of the laser energy with the medium produces a coherent light beam which may be manipulated in the same manner as any other coherent light source (1:2). As a spectroscopic diagnostic tool, CARS is extremely useful in harsh or delicate environments where probes would be destroyed or would disturb the environment. Since the lasers interact with the medium nonintrusively, the CARS process is particularly applicable to performing diagnostics on flames or plasmas. The Air Force has been interested in this technique since it may be used to measure gas species concentrations and temperatures of jet engine exhaust which can aid in the development of alternate fuels as well as

cleaner, more efficient engines (2:1).

The main purpose of this thesis was to incorporate significant improvements into an existing CARS system to increase the system capability and accuracy and to demonstrate the increased accuracy by measuring the frequency shifts of the anti-Stokes lines of molecular hydrogen. Active frequency stabilization of the Ar-ion and dye lasers and the suppression of almost all noise generated by laser scatter by replacing two mirrors with Pellin-Broca prisms allowed measurements of frequency shift coefficients to three significant digits. This represents at least an order of magnitude improvement over any other previously reported method.

The study of hydrogen gas serves as a foundation of molecular physics because H_2 is the lightest and simplest molecule found in nature, and knowledge of its molecular kinetic and gas dynamic properties provides insight into understanding similar properties in more complex molecules. Additionally, in order to use hydrogen as a component in fuels or in laser systems, accurate measurements of its molecular parameters must be available. The measurements undertaken in this study could probably be justified on this basis alone, but with the advent of the Strategic Defense Initiative (SDI), there is a practical application of the frequency shift phenomenon important to both the Air Force and SDI. Raman scattering is currently being investigated as a means of shifting the frequency on an excimer laser,

and it is also being studied as a method of combining laser beams. Both of these processes are deemed to be critical links in the realization of the high-energy laser weapons which are presently being developed for tactical and strategic applications. Since H_2 is one of the best Raman scatterers of all gases, it is a prime candidate for use in both of these technologies. Accurate data on hydrogen's fundamental molecular parameters, such as its Raman linewidths and frequency shift coefficients, is essential to the successful integration of the Raman scattering techniques into the development of the optimum laser weapons system.

Chapter II presents a derivation of the pressure broadened CARS lineshape and explains the frequency shift phenomenon. Chapters III and IV show the experimental apparatus used for the Ar-ion frequency stabilization and the production and collection of the anti-Stokes signal, respectively. Chapter III also contains a brief description of the theory of the servo control system implemented in this study. Chapter IV describes the procedure used to collect the frequency shift data. In chapter V, the data obtained is presented and the frequency shift coefficients determined from it are compared to those of other researchers. Finally, chapter VI contains the conclusions in addition to recommendations for continued research in this area.

II. Theory

The CARS process is a third-order non-linear Raman scattering effect, and the lineshape of the CARS photons is highly dependent on the pressure of the medium. The medium in this study, molecular hydrogen, exhibits the effects of a medium in the pressure broadened regime over the range of pressures investigated. When the pressure of the hydrogen is varied, one of the effects is a significant shift of its anti-Stokes frequencies. This chapter presents a derivation of the pressure-broadened CARS lineshape and an explanation of the frequency shift phenomenon.

Generation of CARS Photons

To drive hydrogen gas to emit a CARS photon, a single mode Ar-ion laser (pump beam) at a frequency of 20492 cm^{-1} (4880 \AA) will excite the molecules to a virtual energy level. A tunable dye laser (Stokes beam) operating at 16331 cm^{-1} or 16343 cm^{-1} (6123 \AA and 6119 \AA) for the Q(1) and Q(2) transitions, respectively, focussed collinearly with the Ar-ion laser will stimulate the molecule down to some vibrational level higher in energy than the ground state. The pump beam will then reexcite the same molecule to a second virtual state higher than the first, and the relaxation of the molecule back to the ground state causes

the emission of a coherent anti-Stokes photon where the angular frequencies of the various photons are related by

$$\omega_{AS} = 2\omega_p - \omega_s \quad (1)$$

(ω_{AS} is the anti-Stokes frequency, ω_p is the pump frequency, and ω_s is the Stokes frequency). The process is shown schematically in figure 1.

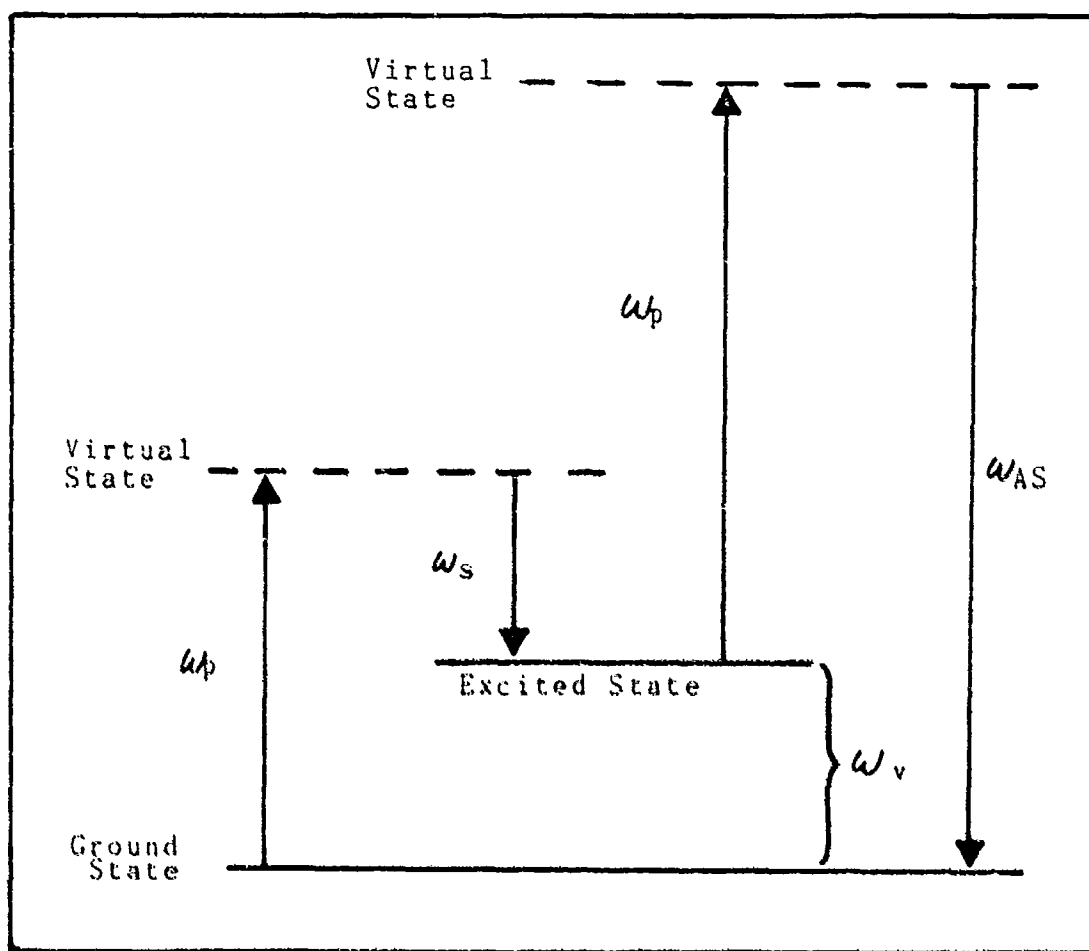


Figure 1. The generation of anti-Stokes photons.

When a vibrating gas molecule undergoes an elastic collision, the frequency of the emitted photon is shifted. The amount of shift is largely dependent upon the pressure

of the gas, but it is also dependent upon the optical cross section of the molecule. The anti-Stokes lines of H_2 exhibit a relatively strong, measurable frequency shift. To understand these effects, the theory of the generation of CARS photons will be presented along with a description of the cause of pressure induced frequency shifts.

Third-Order CARS Susceptibility

The following derivation is a synthesis of material contained in several sources, (1:4-10; 3:90-97). The generalized polarization of a medium responding to an electromagnetic wave is given by

$$\hat{P} = \epsilon_0 \chi^{(1)} E + \epsilon_0 [\chi^{(2)} E + \chi^{(3)} E^2 + \dots] \hat{E} \quad (2)$$

where \hat{P} is the polarization, \hat{E} is the electric field vector, ϵ_0 is the permittivity of free space, and χ is the medium susceptibility. This can be represented as the sum of a linear and non-linear polarization:

$$\hat{P} = \hat{P}^L + \hat{P}^{NL} \quad (3)$$

where

$$\hat{P}^L = \epsilon_0 \chi^{(1)} \hat{E} \quad (4)$$

and

$$\vec{P}^{NL} = \epsilon_0 [\chi^{(2)} E + \chi^{(3)} E^2 + \dots] \vec{E} \quad (5)$$

The polarization responsible for CARS arises when the field

$$E(z,t) = A_p \exp[i(k_p z - \omega_p t)] + A_s \exp[i(k_s z - \omega_s t)] \\ + \text{complex conjugate} \quad (6)$$

is injected into the third-order, non-linear polarization term:

$$P^{(3)} = \epsilon_0 \chi^{(3)} E^3 \quad (7)$$

The CARS polarization term is identified as

$$P_{\text{CARS}} = 3\epsilon_0 \chi^{(3)} A_p^2 A_s^* \exp\left\{i \left[(2k_p - k_s)z + (2\omega_p - \omega_s)t \right]\right\} \quad (8)$$

where $2\omega_p - \omega_s$ is the anti-Stokes frequency providing

$$\omega_p - \omega_s = \omega_v \quad (9)$$

(ω_v is a vibrational frequency of the molecule). To find the third-order susceptibility classically, the interaction energy, \mathcal{H}_I , between the medium and the electromagnetic wave must be used:

$$\mathcal{H}_I = -\frac{1}{2} \vec{P} \cdot \vec{E} = -\frac{1}{2} N(\alpha \vec{E}) \cdot \vec{E} \quad (10)$$

(α is the polarizability of the medium and N is the number density of molecules). The polarizability can be expressed as a Taylor series in terms of the internuclear displacement, q , to give

$$\mathcal{H}_I = -\frac{1}{2} N(\alpha_0 + q \frac{\partial \alpha}{\partial q} + \dots) E^2 \quad (11)$$

The non-linear polarization of the medium is

$$P^{NL} = -\frac{\partial \mathcal{H}_I}{\partial E} = Nq \frac{\partial \alpha}{\partial q} E \quad (12)$$

Since the response of the medium can be modeled mechanically as a collection of simple harmonic oscillators, the force, F , exerted by the electric field on the molecules and the subsequent equation of motion are

$$F = -\frac{1}{N} \frac{\partial \mathcal{H}_I}{\partial q} = \frac{1}{2} \frac{\partial \alpha}{\partial q} E^2 \quad (13)$$

and

$$\frac{\partial^2 q}{\partial t^2} + \Gamma \frac{\partial q}{\partial t} + \omega_v^2 q = \frac{F}{m} = \frac{1}{2m} \frac{\partial \alpha}{\partial q} E^2 \quad (14)$$

respectively. For an electric field of the form

$$E = A_p \exp[i(k_p z - \omega_p t)] + A_s \exp[i(k_s z - \omega_s t)] + \text{c.c.} \quad (15)$$

(i.e. comprised of the pump and Stokes laser beams), as a trial solution, let

$$q = Q \exp\{i[(k_p - k_s)z + (\omega_p - \omega_s)t]\} + \text{c.c.} \quad (16)$$

which, when substituted into (14), yields

$$q = \frac{1}{m} \frac{\partial \alpha}{\partial q} \frac{A_p A_s^* \exp\{i[(k_p - k_s)z - (\omega_p - \omega_s)t]\}}{\omega_v^2 - i\Gamma(\omega_p - \omega_s) - (\omega_p - \omega_s)^2} \quad (17)$$

By substituting (17) into (12), the first form of the non-linear polarization is found:

$$P^{NL} = \frac{N}{m} \left(\frac{\partial \alpha}{\partial q} \right)^2 A_p^2 A_s^* \frac{\exp \{ i [(2k_p - k_s)z - (2\omega_p - \omega_s)t] \}}{\omega_v^2 - i\Gamma(\omega_p - \omega_s) - (\omega_p - \omega_s)^2} \quad (18)$$

Equating (18) with (8) yields the third order susceptibility:

$$\chi^{(3)} = \frac{N}{3m \epsilon_0} \left(\frac{\partial \alpha}{\partial q} \right)^2 \frac{1}{\omega_v^2 - (\omega_p - \omega_s)^2 - i\Gamma(\omega_p - \omega_s)} \quad (19)$$

To make the equation more manageable, a simple approximation may be made. Since $\chi^{(3)}$ is only significant when $\omega_p - \omega_s \cong \omega_v$, the denominator may be expressed as

$$2\omega_v[\omega_v - (\omega_p - \omega_s)] - i\Gamma\omega_v \quad (20)$$

and the susceptibility becomes:

$$\chi^{(3)} = \frac{N}{6m \epsilon_0 \omega_v} \left(\frac{\partial \alpha}{\partial q} \right)^2 \frac{1}{\omega_v - (\omega_p - \omega_s) - i\frac{\Gamma}{2}} \quad (21)$$

The real intensity profile is proportional to the square of the susceptibility:

$$I(\omega) \propto |\chi^{(3)}(\omega)|^2 \quad (22)$$

which leads to a Lorentzian line profile:

$$I(\omega) = I_0 \frac{\left(\frac{\Gamma}{2}\right)^2}{[\omega_v - (\omega_p - \omega_s)]^2 + \left(\frac{\Gamma}{2}\right)^2} \quad (23)$$

Γ , the damping constant, is the fullwidth at half maximum of the intensity profile.

Frequency Shift

When the hydrogen molecule suffers a collision during the emission of an anti-Stokes photon, the frequency of the photon depends on the potentials of the molecules at the time of the transition. Because there is a distribution about some mean molecular separation, \bar{R} , which is a function of both pressure and temperature, there is also a distribution of potentials and therefore a distribution of frequency shifts. Elastic collisions perturb the phases of oscillation of the colliding molecules and not their amplitudes. The sum of all the random phase shifts leads to a frequency shift of the pressure broadened CARS line. The pressure broadened, line-shifted profile for the anti-Stokes transition becomes

$$I(\omega) = I_0 \frac{(N\bar{v}\sigma_b)}{[\omega_v - (\omega_p - \omega_s) - N\bar{v}\sigma_s]^2 + (N\bar{v}\sigma_b)^2} \quad (24)$$

where \bar{v} is the mean velocity of the molecules and σ_b and σ_s are the real and imaginary optical cross sections, respectively, and the frequency shift from the line center is seen to be

$$\Delta\omega = N\bar{v}\sigma_s \quad (25)$$

In this study, the Stokes frequencies were used to determine the line shifts of the anti-Stokes line. The frequencies can be expressed as a 'virial-type' expansion in the powers

of density ρ , (4:1102):

$$[\nu_{Q(J)}]_{\rho} = \nu_{Q(J)} + a_j \rho + b_j \rho^2 \quad (26)$$

where a_j and b_j are the expansion coefficients to be determined from the data.

III. Frequency Stabilization of the Argon-ion Laser

In order to make accurate measurements of the frequency shifts of the anti-Stokes lines of hydrogen on the basis of Stokes frequency measurements, a stable, fixed pump beam frequency is needed. Although operating in a single cavity mode, the argon-ion laser frequency will drift as the cavity and the single-mode etalon undergo thermal expansion and contraction, mechanical vibration, and index of refraction changes with air pressure fluctuations. To insure that the laser remained at the same frequency throughout the measurements, it was stabilized using a feedback control system. The method involves frequency modulating the laser output and locking the laser to a suitable, stable reference.

Laser Frequency Drift

The importance of laser frequency stabilization is evident from an examination of elementary laser theory (3:291-296). Assuming that the laser medium of a gas laser fills the entire volume between the mirrors, the longitudinal frequencies supported by the cavity are given by:

$$\nu = \frac{q c}{2 n L} \quad (27)$$

where n is the index of refraction of the gas, L is the cavity length, and q is an integer. The derivative of (27) determines the change in frequency with changes in cavity length and index of refraction;

$$-\frac{\Delta \nu}{\nu} = \frac{\Delta n}{n} + \frac{\Delta L}{L} \quad (28)$$

The linear thermal expansion of the cavity is given by:

$$\frac{\Delta L}{L} = \alpha \Delta T \quad (29)$$

where α is the coefficient of thermal expansion, and the change in the index of refraction of a gas with pressure variation is

$$\frac{\Delta n}{n} = \frac{\Delta p}{p} \quad (30)$$

For a cavity 1 m in length (approximate length of a Spectra Physics Model 165 Ar-ion Laser), a temperature change of 1 K in an quartz spacer ($\alpha = .5 \times 10^{-6}/K$), and a pressure change of 3 mbar (1 mbar = .75 Torr), the change in frequency of an argon 4880 Å (6.15×10^{14} Hz) laser line is approximately 395 MHz. Since the anti-Stokes frequency shifts are on the order of .001 cm^{-1} or 30 MHz, it is clear that a stability of about 10 MHz is needed to attain the desired accuracy for the measurements.

Phase Sensitive Detection

The theory of FM sideband phase sensitive detection described below was presented by Hall et. al (5:99-104) in their observation of the lineshapes of subdoppler resonances. A frequency modulated field of the form

$$E = E_0 \sin(\Omega t + \beta \sin \omega t) \quad (31)$$

(Ω is the optical carrier frequency, ω is the modulation frequency, and β is the modulation index) can be expressed in terms of its Fourier frequency components;

$$E = E_0 \left[\sum_{n=0}^{\infty} J_n(\beta) \sin(\Omega + n\omega)t + \sum_{n=1}^{\infty} (-1)^n J_n(\beta) \sin(\Omega - n\omega)t \right] \quad (32)$$

When the modulation index β is much less than 1, as is the case in this experiment, the Fourier spectrum is closely approximated by the carrier frequency (Ω) term and the two first-order sideband ($\Omega \pm \omega$) terms. The field reduces to

$$E = E_0 \left[J_0(\beta) \sin \Omega t + J_1(\beta) \sin(\Omega + \omega)t - J_1(\beta) \sin(\Omega - \omega)t \right] \quad (33)$$

A photodetector responds to light intensity, $\langle E^2 \rangle$ where $\langle \rangle$ represents a time average over optical frequency:

$$E^2 = J_0^2(\beta) \sin^2 \Omega t + J_0(\beta) J_1(\beta) \sin \Omega t \sin(\Omega + \omega)t - J_0(\beta) J_1(\beta) \sin \Omega t \sin(\Omega - \omega)t + \dots \quad (34)$$

Equation (34) shows that the two first-order sideband terms are equal in magnitude but opposite in sign and therefore the time-averaged quantities exactly cancel each other. If the balance between the two sidebands is disturbed, for example, by transmission through a frequency sensitive element (a Fabry-Perot etalon in the case of this experiment), the intensity becomes modulated at the modulation frequency. As the cavity changes (and with it the carrier frequency), the Fourier spectrum is tuned across the Fabry-Perot resonance peak. The output of the photodetector is an AC signal at the modulation frequency whose amplitude is a dispersion curve corresponding to the derivative of the Fabry-Perot peak (See Figure 2). In the

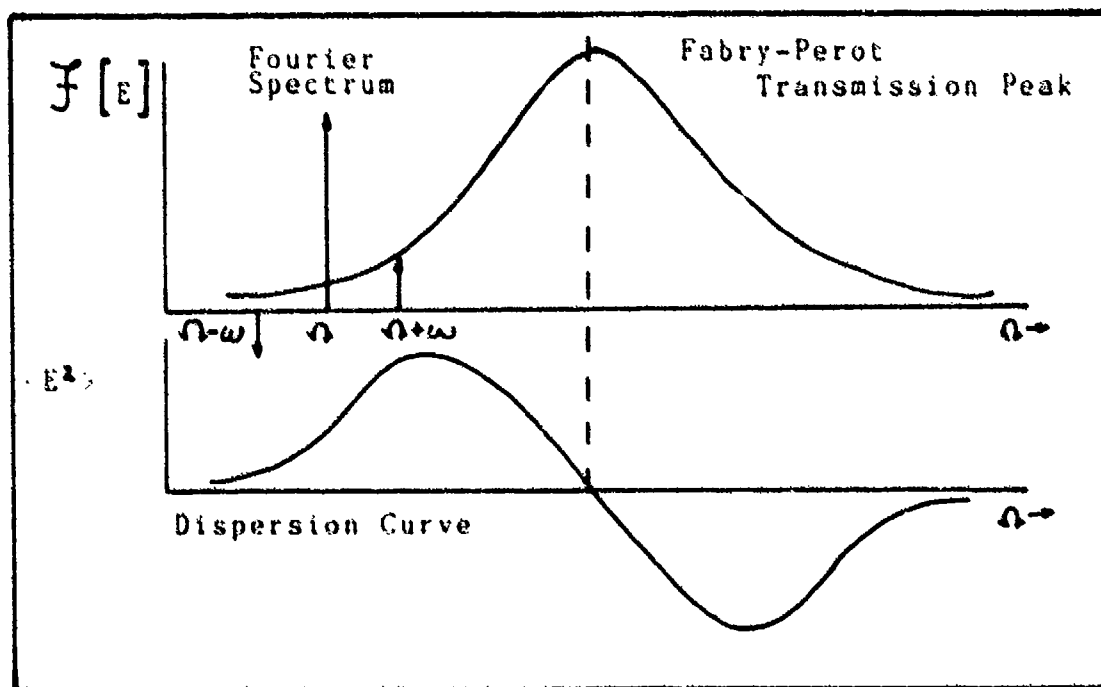


Figure 2. Dispersion curve produced by tuning the Fourier frequency spectrum of a frequency modulated signal across a Fabry-Perot transmission peak.

vicinity of the transmission peak, the photodetector produces a bipolar signal which the lockin amplifier can use as an error signal. The lockin amplifier detects the amplitude of the error signal and passes it to a high-voltage operational amplifier which drives a piezoelectric transducer mounted on the laser mirror. The movement of the PZT adjusts the laser cavity length such that the laser frequency remains at the Fabry-Perot transmission peak frequency (i.e. the zero of the dispersion curve).

Servo Control System

To implement phase sensitive detection to frequency-stabilize a laser, an invariant reference and a servo loop, which can detect differences, Δ , between the laser frequency and the reference and return Δ to zero as ν_{laser} fluctuates, are needed. For this experiment, the reference was a transmission maximum of a thermally stabilized semi-confocal, Fabry-Perot etalon. An EG&G PARC Model 5301 Lock-in amplifier and a Burleigh PZ-70 high voltage operational amplifier were used in the servo control circuit (See Figure 3).

Although the pump wavelength for the anti-Stokes transition of H_2 is the 4880 \AA Ar^+ laser line, the reflectivity of the reference etalon mirror coatings, optimized for the red portion of the spectrum, did not

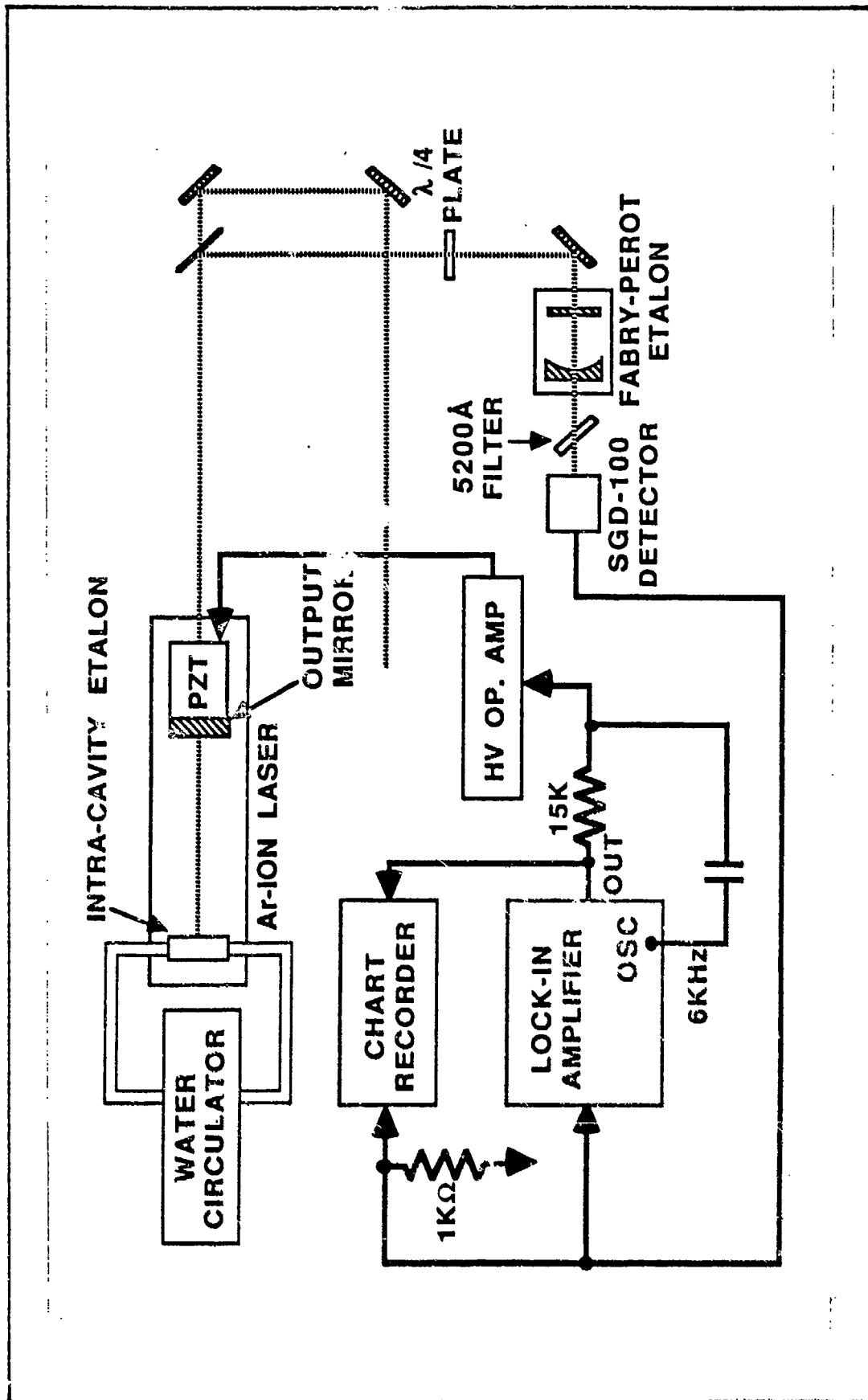


Figure 3. Schematic diagram of frequency stabilization system.

extend to that wavelength. Consequently, the coatings were not sufficiently reflective at 4880 Å to produce sharp, distinct interference peaks but were still reflective enough at the 5145 Å Ar⁺ line to generate the needed transmission maxima. To remedy this problem, the single-wavelength prism/mirror of the Ar-ion laser was replaced with a multilayer reflector which enabled the laser to produce enough power at 4880 Å to generate the CARS signal while simultaneously emitting the 5145 Å line needed for use with the reference etalon. An intra-cavity etalon and aperture in the laser limited all wavelengths to a single longitudinal and transverse mode, and since the frequency drifts caused by cavity variations affect all lines, stabilizing the 5145 Å line stabilizes all output wavelengths. It was found, however, that the laser's intra-cavity etalon transmission peaks underwent enough thermal drift to cause mode hopping which consequently unlocked the servo loop. The drift was remedied by flowing 25°C temperature-controlled water through the etalon mount. This provided the stability needed to prevent mode hopping without introduction of significant mechanical vibration from the water flow which had been feared.

The output mirror of the Ar-ion laser was mounted on a piezoelectric transducer which was driven by the op amp and modulated at 6 kHz using the internal oscillator output of from the lock-in amplifier. A portion of the laser light

was split from the main beam and sent to the Fabry-Perot reference etalon. In order to prevent the retro reflection from causing instabilities in the laser output, a quarter-wave plate was used to rotate the polarization of the reflection by 90° . The 5145 \AA line was separated from the beam by an angle-tuned 5200 \AA bandpass filter. The etalon transmission maxima were detected by a PIN diode photodetector, and the laser frequency was locked onto the highest transmission peak. To monitor the frequency lock, the signal from the photodetector was also sent to a chart recorder. The locking scheme resulted in a frequency stabilization of approximately 8 MHz which permitted extremely accurate resolution of the anti-Stokes frequency shifts.

IV. Experimental Procedure

The generation and detection of the CARS signal in hydrogen gas requires precision alignment of two laser beams along with several dozen optical and electronic components. Once the experimental apparatus has been set and the anti-Stokes signal found, a careful and painstaking procedure must be followed to refine the alignment in order to maximize the signal so that the anti-Stokes frequency shift can be identified and quantified. In this chapter, the functions of the critical optics and electronics will be explained along with the procedure followed to collect experimental data.

Experimental Apparatus

Figure 4 shows a schematic diagram of the experimental set-up. A Spectra Physics Model 171 Ar-ion laser emitting 13 W of multiline output was used to pump the rhodamine 6G or rhodamine RB laser dyes of a Coherent CR-699-21 ring dye laser. The dye laser alignment was optimized to produce between 200 and 500 mW of single-mode power at 16331 cm^{-1} and 16343 cm^{-1} which are near the Stokes frequencies of the Q(1) and Q(2) transitions of H_2 , respectively. The polarization of the beam was rotated 90° to horizontal by a periscope mirror to match the polarization of the second Ar-

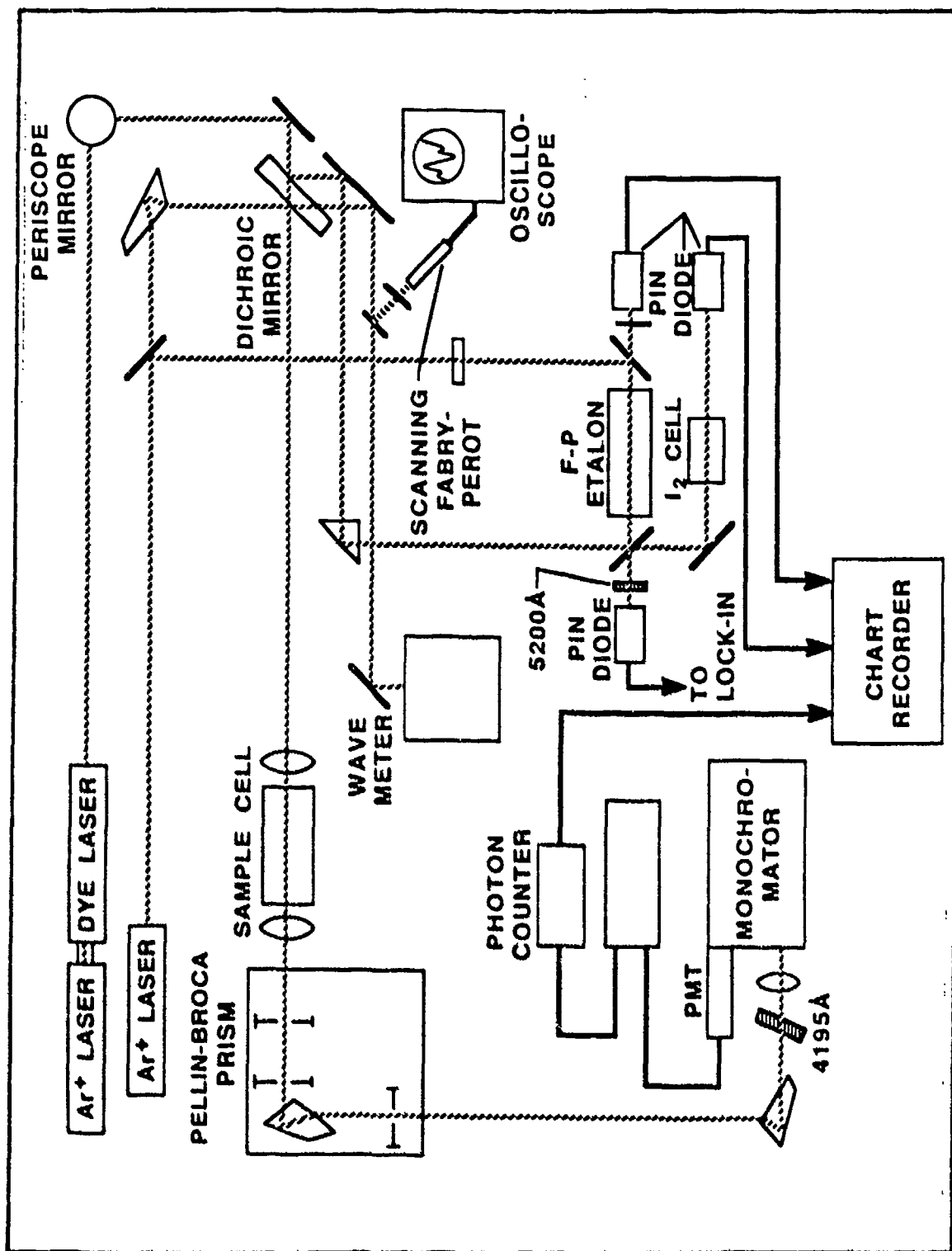


Figure 4. Schematic diagram of experimental apparatus.

ion laser, a Spectra Physics Model 165, whose polarization was also rotated to horizontal to reduce reflection losses off the Pellin-Broca prism surfaces. To pump the hydrogen gas, the Model 165 Ar-ion laser emitting principally 4880 Å and 5145 Å at approximately 1.3 W of multiline power was directed collinearly with the dye beam using a dichroic mirror. The dichroic mirror is coated to reflect the 4880 Å and 5145 Å light while passing the dye laser wavelengths (~6100 Å). A long-pass low-fluorescence 4200 Å filter was placed in the Ar beam to pass the longer wavelengths but absorb the higher frequency Ar plasma tube radiation which is in the vicinity of the anti-Stokes frequency and much more intense than the signal and consequently would swamp it. (With the incorporation of the Pellin-Broca prisms described below, the filter was no longer needed to block the high frequency radiation from the plasma tube, but it was still used as the beam splitter which sent the beam to the Fabry-Perot etalon for frequency stabilizing the Ar-ion laser.) The two beams were focussed into a high-pressure gas cell with a 10 cm focal length lens in order to create a higher power density in the focal volume than the raw beams and thereby enhance the signal gain. As the beams exited the cell, they were refocussed into the dispersion system which consisted three apertures and a Pellin-Broca prism mounted on a micrometer controlled rotation stage. The apertures gave the system enough directionality to perform an

approximate wavelength calibration for the throughput. Calibrated using the Ar-ion laser lines and the Hg 4308 Å line, the prism served to separate the anti-Stokes beam from the laser beams while bending the beam path 90°. Once the anti-Stokes line was separated, it was passed through an angle-tuned, 4195 Å band-pass filter, to eliminate the majority of the laser scatter, and then focussed onto the entrance slit of a Jarrel-Ash 1/2-meter monochromator. In an extremely successful attempt to reduce the amount of the scattered Ar-ion light incident upon the monochromator slit, two of the mirrors were replaced with Pellin-Broca prisms to separate the 4880 Å line from the broadband output and also to separate any remaining high frequency radiation generated by the Ar plasma from the anti-Stokes signal. The result was a background noise of 20 to 30 counts per second which was equal to the photomultiplier tube dark count. With the monochromator diffraction grating adjusted to select the anti-Stokes line (4060 Å), an RCA 8850 photomultiplier tube controlled by EG&G PARC Models 1121a and 1112 discriminator unit and photon counter digitally counted the incident anti-Stokes photons and sent the analog output to a chart recorder.

To perform the beam diagnostics, the two reflections of the dye laser from the dichroic mirror were intercepted by a mirror and directed into a subset of optics. Part of the beam was split and sent through a 5300 Å long-pass filter

into a scanning Fabry-Perot spectrum analyzer. The filter blocked the much stronger argon wavelengths while passing the dye beam. The spectrum analyzer was connected to an oscilloscope which allowed the scanning process of the dye laser to be monitored to insure a smooth scan without mode hopping. The remainder of the first beam was sent into a Burleigh WA-10 wavemeter which displayed the dye laser frequency to $\pm .01 \text{ cm}^{-1}$. The wavemeter was not accurate enough to display the exact Stokes frequency, but it did serve to approximate the Stokes frequency range scanned while also identifying the frequencies of the I_2 absorption peaks. Because the reflection from the second surface of the dichroic mirror was only slightly displaced from the primary beam, a right-angle prism was used to steer it into the semi-confocal Fabry-Perot etalon and I_2 cell. The beam was nearly mode-matched to the Fabry-Perot to generate a distinguishable linear frequency marker on the chart recorder while the dye laser was scanned. The dye laser throughput of the Fabry-Perot etalon passed through a long-pass 5700 \AA filter, to block an Ar reflection, and then onto a PIN diode connected to the chart recorder. The final leg of the dye beam was sent through an I_2 cell and onto another PIN diode. Iodine has a large number of absorption peaks and those peaks produced by the dye laser scan served as an absolute frequency reference. From the peaks, the Stokes frequency and subsequently the anti-Stokes frequency and

line shift could be determined to $\pm .001 \text{ cm}^{-1}$.

Data Collection

The process of finding and recording the anti-Stokes signal, although not difficult, required iterative adjustments to maximize the signal. After the beams had been roughly collinearly aligned and the laser power peaked at the desired wavelengths, the dye laser was scanned either manually or electronically near the predicted Stokes frequency. Once a signal had been positively identified, the dye laser was parked on the frequency of maximum signal and the optics were tuned while watching the chart recorder and the photon counter's digital display. The Pellin-Broca prism, the 4195 \AA bandpass filter and the monochromator were adjusted first. Then the beam overlap was corrected followed by a fine adjustment of the dispersion system and detection system. One or two iterations of this process maximized the the signal to approximately 200 to 6000 counts per second depending on the H_2 line observed and the gas pressure. After the Pellin-Broca prisms were substituted for the mirrors, count rates as high as 25,000 were achieved for the Q(1) line. With the entire system optimized, it remained set throughout the gas pressure variations. For pressures ranging from 2 atmospheres up to 40 atmospheres, the dye laser was scanned electronically over 10-15 GHz to

include several I_2 absorption peaks along with the anti-Stokes line. Two scans were taken at each pressure to develop a statistical base and a confidence level in the validity of the measurements. If, when compared to each other, the peaks of the two scans coincided, the measurements were continued at the next pressure. The three pens of the chart recorder graphically printed on a single sheet all the data needed for the determination of the frequencies and line shifts.

V. Data and Analysis

Measurements were made on the Q(1) and Q(2) transitions of H_2 because they are hydrogen's two strongest Q-branch transitions. Measurements of the Q(0) and Q(3) lines were also attempted, but their weak signals were buried under the noise generated by photon statistics so no usable results could be extracted from the data. H_2 was selected because its transitions are comparatively strong and the frequency shifts are significant. Additionally, hydrogen constants have been well documented, so many published results exist for comparison. This chapter presents the data collected followed by an analysis of it. The calculated frequency shift coefficients are then compared to those reported by other researchers.

Data

As stated in the previous chapter, all the information needed to determine frequency shift was recorded on a single sheet from the strip chart recorder. Data was gathered at 2, 3, 5, 8, 10, 15, 20, 30, and 40 atmospheres with photon counts ranging from 600-6000 counts per second for Q(1) and 150-350 cps for Q(2). The Q(1) measurements were taken before the Pellin-Broca prisms were used in the experimental apparatus, so the background count for those measurements

was approximately 200-250 cps while the background for the Q(2) measurements with the prisms in the system was 20-30 cps. Because of the difference in background, the signal-to-noise ratio was between 10 and 30 for both lines. Figures 5 and 6 show typical scans produced by the recorder

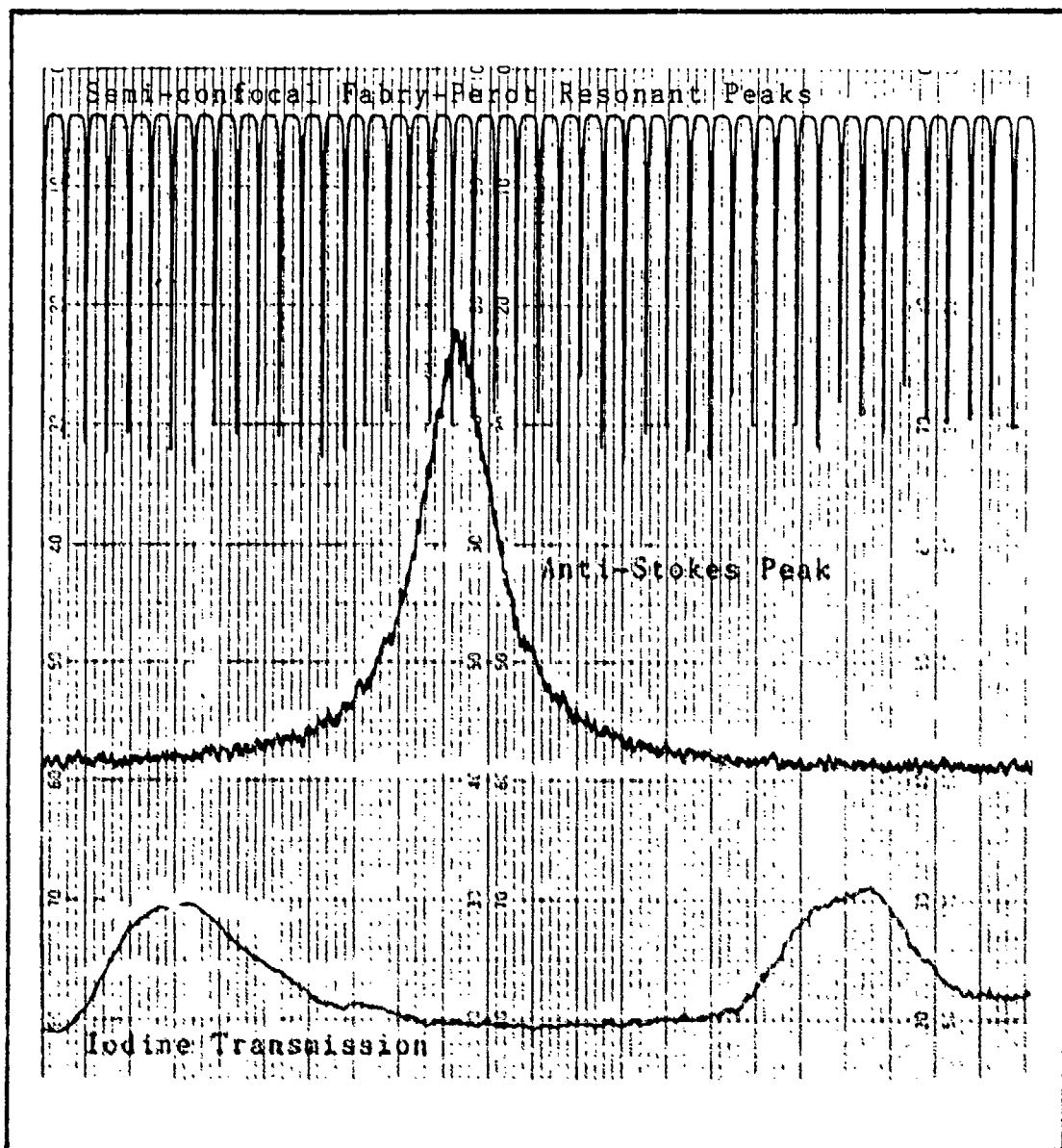


Figure 5. Sample scan of Q(1) transition at 10 atmospheres.

including the anti-Stokes peak, the I_2 absorption peaks, and the Fabry-Perot transmission peaks. Figure 5 is an example of a Q(1) transition at 10 atmospheres and figure 6 shows a Q(2) transition at 5 atmospheres.

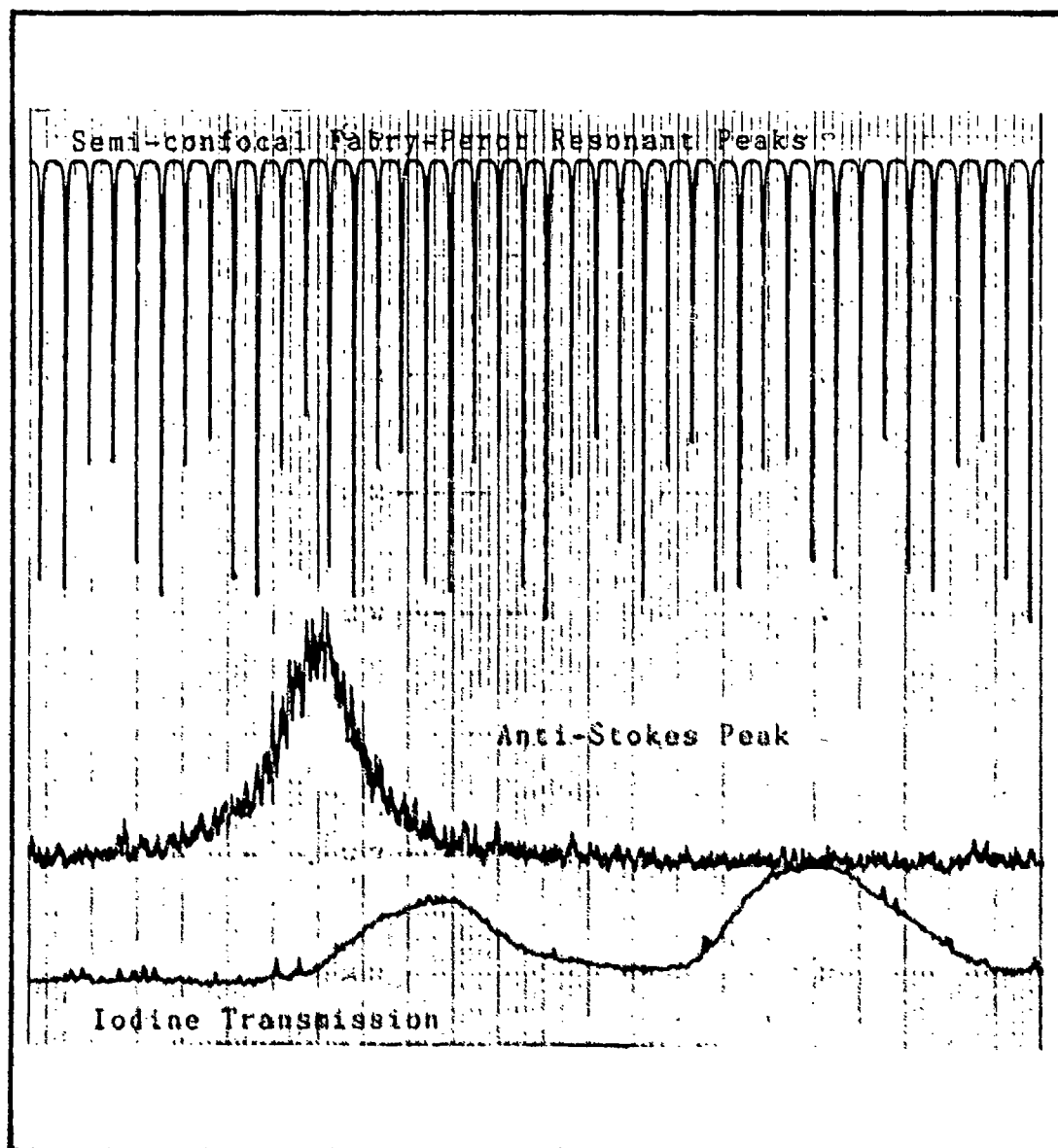


Figure 6. Sample scan of Q(2) transition at 5 atmospheres.

Once the raw data had been collected, hard numbers had to be extracted from the chart recordings. The most visibly symmetric I_2 absorption peak was chosen as the reference for all runs of the same transition. Symmetry in the I_2 peak is important because the center of gravity of an asymmetric absorption peak is impossible to distinguish without information about the hyperfine structure and therefore an error is introduced into the absolute frequency measurement. For this experiment, the relative frequencies were critical in calculating the frequency shift coefficients rather than the absolute frequencies. The I_2 frequency was chosen to be the midpoint of the peak's fullwidth at half maximum (FWHM) and the error in this position from scan to scan was only $\pm 0.0008 \text{ cm}^{-1}$. The anti-Stokes peak frequency was also determined by identifying the midpoint of the FWHM of the anti-Stokes line. The actual Stokes frequency was established by counting the number of Fabry-Perot resonant peaks between the I_2 peak and the anti-Stokes peak, multiplying it by the free spectral range of the interferometer ($124 \pm 4 \text{ MHz}$), and adding or subtracting as appropriate from the I_2 absorption peak frequency. Tables I and II contain the Stokes frequencies for the Q(1) and Q(2) transitions, respectively. The error in the absolute frequencies is approximately $\pm 0.004 \text{ cm}^{-1}$, due mainly to the uncertainty of the I_2 frequency, but only $\pm 0.001 \text{ cm}^{-1}$ for the relative frequency measurements.

Table I

Stokes Frequencies of the Q(1) Transition

Pressure (atm)	Stokes Frequency (cm^{-1})	Pressure (atm)	Stokes Frequency (cm^{-1})
2	16331.333	15	16331.375
	16331.336		16331.375
3	16331.339	20	16331.389
	16331.340		16331.391
5	16331.346	30	16331.415
	16331.346		16331.416
			16331.418
8	16331.353	40	16331.444
	16331.354		16331.446
10	16331.361		
	16331.361		

Table II

Stokes Frequencies of the Q(2) Transition

Pressure (atm)	Stokes Frequency (cm^{-1})	Pressure (atm)	Stokes Frequency (cm^{-1})
3	16343.166	15	16343.183
	16343.167		16343.190
5	16343.170	20	16343.196
	16343.170		16343.197
8	16343.176	30	16343.213
	16343.177		16343.214
10	16343.178		
	16343.180		

Analysis

Because the anti-Stokes and Stokes frequencies are related in terms of the pump frequency which is fixed (Eq.1), only the Stokes frequencies and gas pressures are needed to determine the frequency shift coefficients. Figure 7 is a composite showing the relative frequency shift, line broadening, and variation in intensity of the Q(2) transition occurring at two different pressures. The coefficients were determined by performing both a linear and quadratic fit to the data points using the method of least squares. Although the value of chi-squared was smaller for the quadratic fits than the linear, the coefficient standard deviations were 100 times smaller for the linear fits than the quadratic. Figures 8 and 9 show the linear fits to the data points of the two lines along with the frequency shift data obtained two years earlier by Melton and Toich (1:51, 53, 64, 65) on the same apparatus without the benefit of the frequency stabilization of the Ar-ion laser. These figures not only drastically show the need for frequency stabilization in frequency shift measurements, but they also show the success attained by frequency stabilizing the laser used in this experiment.

Frequency shift coefficients are generally derived from the molecule's vibrational transition frequencies and gas density in units of amagats. In order to compare the

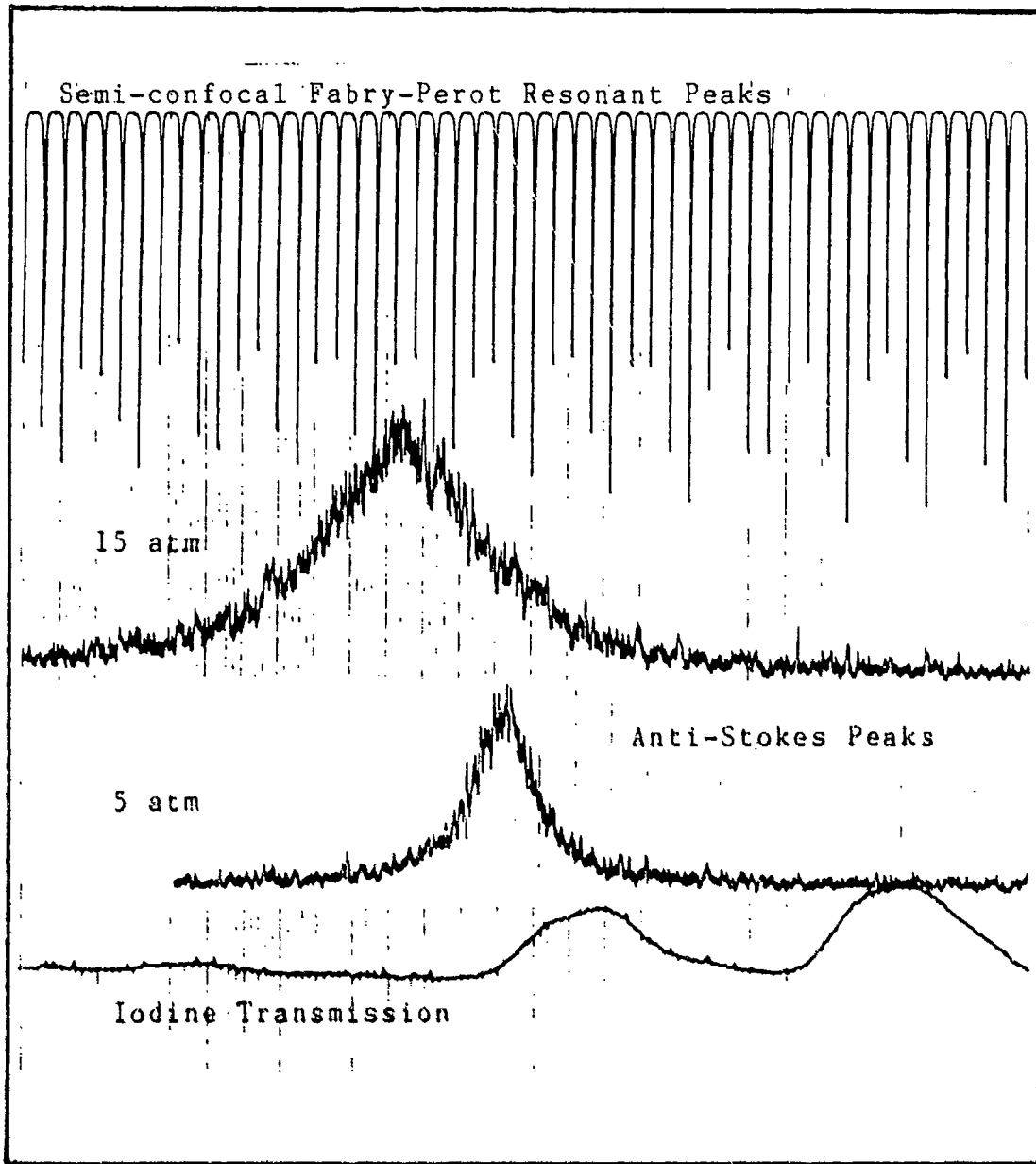


Figure 7. Relative frequency shift, pressure broadened linewidth, and signal intensity of the Q(2) transition at 5 and 15 atmospheres.

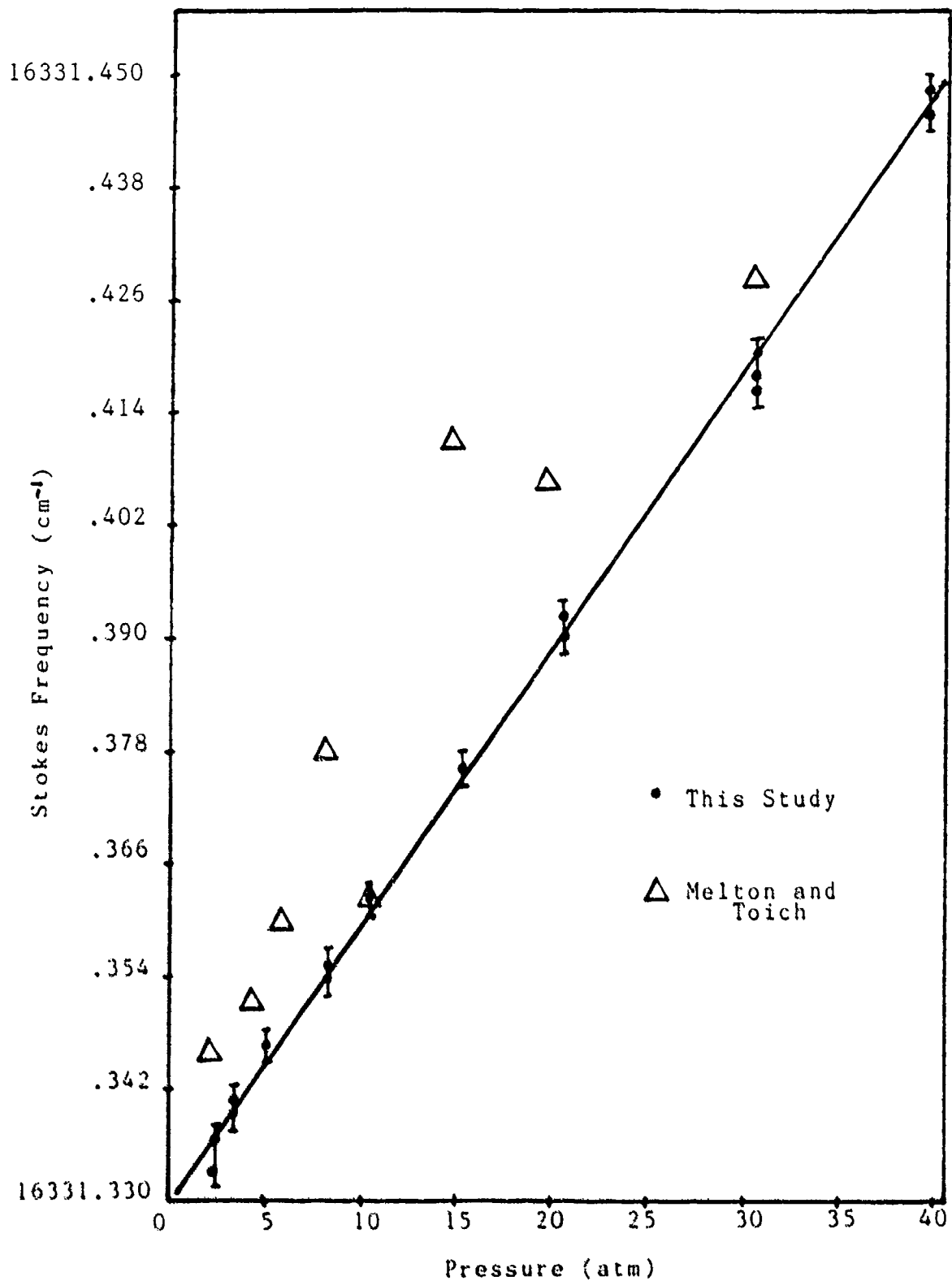


Figure 8. Q(1) frequency shift as a function of pressure.

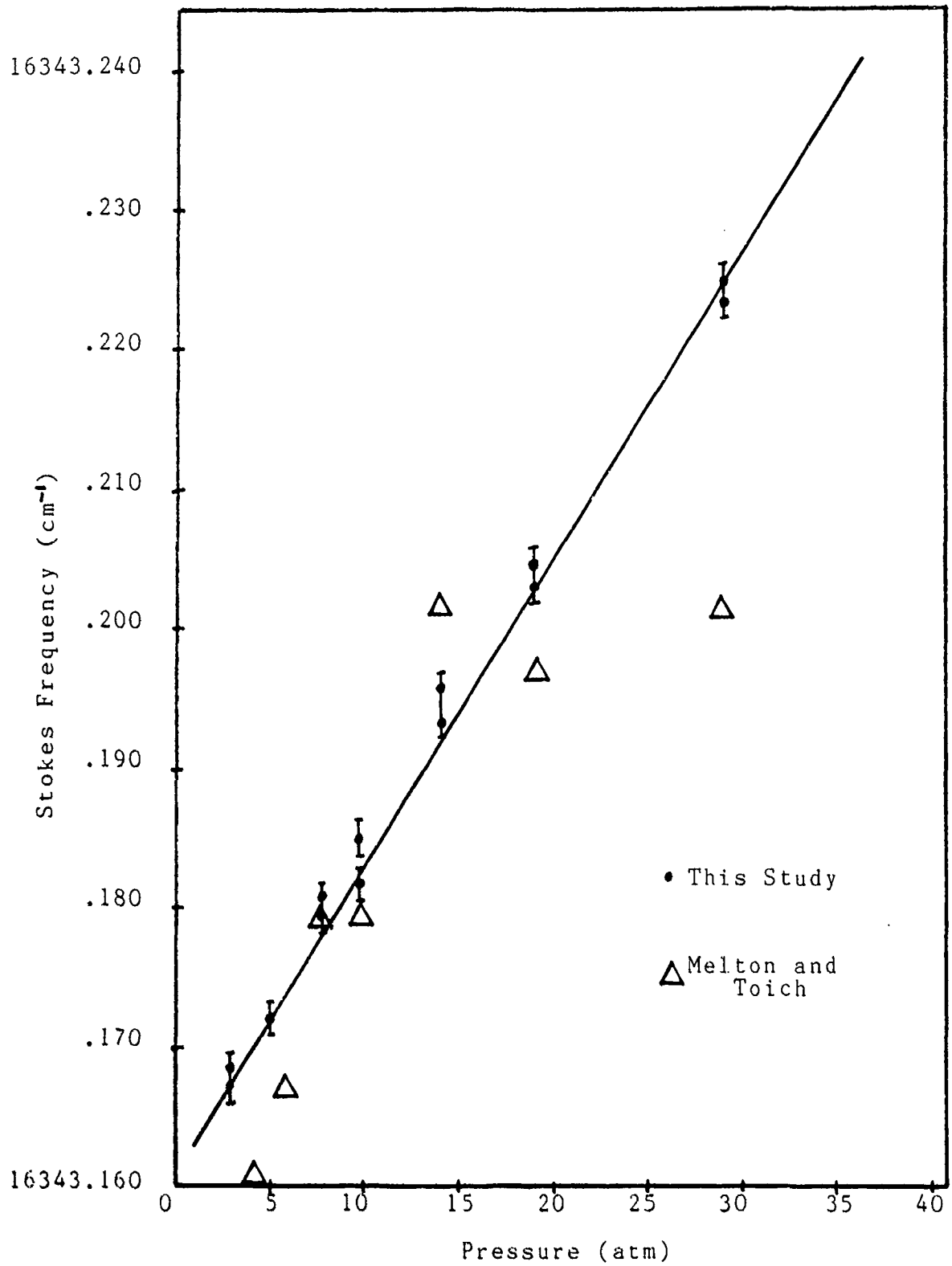


Figure 9. Q(2) frequency shift as a function of pressure.

Table III

Comparison of frequency shift coefficients for the Q(1) Transition

	This Study	Murray and Javan (6:11)	May et.al. (7:1062)	Bragg et.al. (8:1003)	Looi et.al. (4:1105)	Foltz et.al. (9:206,208)
Linear						
a	-3.150 ± .029	-2.5	-	-2.13 ± .14	-3.05 ± .14	-3.18
δ	.0059	7	-	-	-	-
Quadratic						
a	-3.417 ± .099	-3.0	-3.14 ± .15	-	-	-3.25
b	7.3 ± 2.6	4.5	4.86 ± .35	-	-	4.63
δ	.0049	6.3	-	-	-	-

a in units of 10^{-3} cm $^{-1}$ amagat $^{-1}$ b in units of 10^{-6} cm $^{-1}$ amagat $^{-2}$ δ rms error of the fit in units of 10^{-3} cm $^{-1}$

$$[\nu_{Q(J)}]_p = \nu_{Q(J)} + a_j \rho + b_j \rho^2$$

Table IV

Comparison of frequency shift coefficients for the Q(2) Transition

This Study	Murray and Javan (6:11)	May et.al. (7:1062)	Bragg et.al. (8:1003)	Looi et.al. (4:1105)	Foltz et.al. (9:208)
Linear					
a	-1.906 ± .033	-1.35	-	-2.0 ± .1	-2.22 ± .21
δ	.0035	7	-	-	-
Quadratic					
a	-2.13 ± .13	-	-2.07 ± .16	-	-
b	7.8 ± 4.1	-	5.77 ± .37	-	-
δ	.0030	-	-	-	-

a in units of 10^{-3} cm⁻¹ amagat⁻¹

b in units of 10^{-6} cm⁻¹ amagat⁻²

δ rms error of the fit in units of 10^{-3} cm⁻¹

$$[\nu_{Q(J)}]_p = \nu_{Q(J)} + a_j p + b_j p^2$$

coefficients determined in this study with other published results, the coefficients had to be changed to the more generally accepted units. The conversion between atmospheres and gas density is by a proportionality constant: $P_{\text{amagats}} = .9099 P_{\text{atm}}$. Converting Stokes frequency shift coefficients to vibrational frequency shift coefficients is equally as simple: multiplication by -1 (Eq. 9). Even though this study's linear coefficients are an order of magnitude better than other published results, the quadratic coefficients are only of similar accuracy (See Tables III and IV). An examination of the experimental techniques used by the other researchers provides insight into the cause of the differences in accuracies between the linear and quadratic frequency shift coefficients.

The resolution of the CARS system used in this study is limited by the linewidths of the lasers used to generate the anti-Stokes signal. The linewidth of the ring-dye laser is about 1 MHz and the linewidth of the Ar-ion laser although unmeasured is estimated to be around 10 MHz. The combination of the two linewidths (approximately 11 MHz) gives an estimate of the theoretical limit of resolution attainable by the CARS system: $\sim .00037 \text{ cm}^{-1}$, or conservatively $\sim .0005 \text{ cm}^{-1}$. Although the other researchers employed ingenious means of increasing the signal strengths and resolutions (6), in each case, the resolution was limited by their spectrometers. Even with a spectrograph having a grating as large as 25 cm with 1200 lines/mm (the

best grating used by the researchers of the other reported results), the theoretical limit of their resolutions was between $.01 \text{ cm}^{-1}$ and $.05 \text{ cm}^{-1}$ for first order and between $.007 \text{ cm}^{-1}$ and $.03 \text{ cm}^{-1}$ for second order depending on whether they measured vibrational frequencies (emission spectroscopy in AC or DC discharges) or Stokes frequencies (spontaneous Raman spectroscopy), respectively.

Even with resolutions 100 times better for this study than was available to the others, the quadratic coefficients determined in this experiment were still only of comparable or poorer accuracy. This can be understood by noting the pressure ranges over which the measurements were taken. In this study, the maximum pressure used was 40 atmospheres while the other researchers used pressures ranging up to 75, 100, 110, and even 1000 atmospheres (9:204, 8:1000, 6:10, 7:1059). The quadratic nature of the frequency shift becomes much more evident at higher pressures, so as can be seen from tables III and IV, May et.al. achieved the most accurate quadratic coefficients since their experiment took measurements up to 1000 atmospheres. The range of pressures used in this study was a serious limitation on the accuracy of the quadratic frequency shift coefficients. From the accuracy of the linear coefficients determined from this experiment, it is clear that a similar accuracy could be realized simply by increasing the range of pressures over which the measurements can be taken.

VI. Conclusions and Recommendations

The success in implementing significant improvements into an existing CARS apparatus led to the measurement of high-accuracy frequency shift coefficients for the Q(1) and Q(2) transitions of H₂. The frequency stability of the Ar-ion laser proved to be a determining factor in resolving the frequency shifts. Additionally, the incorporation of several Pellin-Broca prisms reduced the laser background noise enough so that count rates as low as 150 cps could still yield acceptable data. The linear coefficients determined in this study were an order of magnitude better than any previously published work, but the quadratic coefficients were of similar or slightly poorer accuracy than the other reported values. The frequency shift coefficients are useful not only in the study of molecular kinetics, but they are also needed for possible application to Raman frequency conversion and beam combination of high-energy excimer lasers for use in Air Force laser weapons systems in connection with the SDI program.

Below are several recommendations for system improvement and suggestions for areas of further related research. An important improvement would be to obtain Fabry-Perot etalon mirrors with an optimal reflectivity in the blue-green range of the spectrum to be used to frequency lock the Ar-ion laser. Not only will this reduce the number

of optical components needed in the system, but it would then allow the laser to be operated at a single line thus increasing its output power by eliminating mode competition among the laser transitions. With this accomplished, the frequency shifts for the H_2 Q(0) and Q(3) transitions could be determined to complete the study of the hydrogen Q-branch frequency shifts. With the increase in power, the absolute anti-Stokes frequencies of deuterium and methane could be determined since the Ar-ion laser frequency could be locked onto the I_2 5145 Å absorption peak. The I_2 absorption peak marks an absolute pump frequency, and from that, the absolute anti-Stokes frequencies can be calculated. To increase the accuracy of the quadratic frequency shift coefficients, the measurements should be taken over a much broader range of pressures. This would mean upgrading the gas-handling system to accommodate higher pressures. Finally, frequency shift measurements could also be done on D_2 and CH_4 or other gases of interest.

Bibliography

1. Melton, 2Lt. David W., and Toich, Capt. Anthony M., Linewidth and Bandwidth Measurements of the Q-Branch of H₂ Using CW Coherent Anti-Stokes Raman Spectroscopy. MS Thesis, School of Engineering, Air Force Institute of Technology (AU), Wright-Patterson AFB, OH, December 1984.
2. Roh, Won B., Coherent Anti-Stokes Raman Scattering of Molecular Gases. AFAPL-TR-77-47, August 1977.
3. Demtröder, Wolfgang. Laser Spectroscopy, New York: Springer-Verlag, 1981.
4. Looi, E.C., Stryland, J.C., and Welsh, H.L., "Pressure Shifts in the Vibrational Raman Spectra of Hydrogen and Deuterium, 315-85K," Canadian Journal of Physics, 56: 1102-1108 (1978).
5. Hall, J.L., Robinson, H.G., Baer, T., and Hollberg, L., "The Lineshapes of Subdoppler Resonances Observable with FM Side-band (Optical Heterodyne) Laser Techniques," Advances in Laser Spectroscopy, New York: Plenum Press, 1983.
6. Murray, J.R. and Javan, A., "Effects of Collisions on Raman Line Profiles of Hydrogen and Deuterium Gas," Journal of Molecular Spectroscopy, 42: 1-25 (1972).
7. May, A.D., Varghese, G., Stryland, J.C., and Welsh, H.L., "Vibrational Frequency Perturbations in the Raman Spectrum of Compressed Gaseous Hydrogen," Canadian Journal of Physics, 42: 1058-1069 (1964).
8. Bragg, S.L., Brault, J.W., and Smith, W.H., "Line Positions and Strengths in the H₂ Quadrupole Spectrum," The Astrophysical Journal, 263: 999-1004 (1982).
9. Foitz, J.V., Rank, D.H., Wiggins, T.A., "Determinations of Some Hydrogen Molecular Constants," Journal of Molecular Spectroscopy, 21: 203-216 (1966).

VITA

Second Lieutenant Mark P. Jelonek was born on 5 January 1963 in Milwaukee, Wisconsin. He graduated from Warren Area High School in Warren, Pennsylvania in 1981. He attended the Pennsylvania State University where he received a Bachelor of Science degree, with highest distinction, in Physics in 1985. He also earned a regular commission in the USAF through the ROTC program and was immediately called to active duty to enter the physics program of the School of Engineering, Air Force Institute of Technology, in May 1985.

Permanent Address: 3945 Barachel Dr.
York, Pennsylvania 17402

REPORT DOCUMENTATION PAGE

1a. REPORT SECURITY CLASSIFICATION UNCLASSIFIED			1b. RESTRICTIVE MARKINGS		
SECURITY CLASSIFICATION AUTHORITY			3. DISTRIBUTION / AVAILABILITY OF REPORT Unlimited		
2b. DECLASSIFICATION / DOWNGRADING SCHEDULE			4. PERFORMING ORGANIZATION REPORT NUMBER(S) AFIT/GEP/ENP/86D-5		
5. MONITORING ORGANIZATION REPORT NUMBER(S)			6a. NAME OF PERFORMING ORGANIZATION Air Force Institute of Technology		
6b. OFFICE SYMBOL (if applicable) AFIT/EN			7a. NAME OF MONITORING ORGANIZATION		
6c. ADDRESS (City, State, and ZIP Code) Wright-Patterson AFB, Ohio 45433			7b. ADDRESS (City, State, and ZIP Code)		
8a. NAME OF FUNDING / SPONSORING ORGANIZATION		8b. OFFICE SYMBOL (if applicable)		9. PROCUREMENT INSTRUMENT IDENTIFICATION NUMBER	
8c. ADDRESS (City, State, and ZIP Code)		10. SOURCE OF FUNDING NUMBERS			
		PROGRAM ELEMENT NO.	PROJECT NO.	TASK NO.	WORK UNIT ACCESSION NO.
11. TITLE (Include Security Classification) Frequency Shift Measurements of the Q(1) and Q(2) Lines of H ₂ Using High Resolution CW Coherent Anti-Stokes Raman Spectroscopy					
12. PERSONAL AUTHOR(S) Mark P. Jelonek, 2nd Lt., USAF					
13a. TYPE OF REPORT MS Thesis		13b. TIME COVERED FROM 6/86 TO 10/86		14. DATE OF REPORT (Year, Month, Day) 1986, 12, 10	15. PAGE COUNT 54
16. SUPPLEMENTARY NOTATION Approved for Public Release LAW 100-17 LYNN E. WOLAVEN 7 April 87 Liaison for Research and Professional Development					
17. COSATI CODES			18. SUBJECT TERMS (Continue on reverse if necessary and identify by block number)		
FIELD	GROUP	SUB-GROUP	Coherent, Anti-Stokes, Raman Spectroscopy		
20	06		Hydrogen, Frequency Shift		
07	04				
19. ABSTRACT (Continue on reverse if necessary and identify by block number) Linear and quadratic frequency shift coefficients were determined for the Q(1) and Q(2) lines of H ₂ using cw Coherent Anti-Stokes Raman Spectroscopy (CARS). The linear coefficients were accurate to three significant digits which is an order of magnitude better than any other published results. The quadratic coefficients were comparable to other reported results because of the range of pressures investigated in this study. Frequency stabilization of the Ar-ion laser allowed accurate measurements of the frequency shifts over a range of 2 to 40 atmospheres. A Fabry-Perot interferometer provided a relative frequency marker and iodine absorption peaks provided an absolute frequency reference. The coefficients determined were compared to those calculated by other researchers using different experimental methods. The high accuracy of the measurements added further credence to the effectiveness of cw CARS as a high resolution spectroscopic tool.					
DISTRIBUTION / AVAILABILITY OF ABSTRACT <input type="checkbox"/> UNCLASSIFIED/UNLIMITED <input checked="" type="checkbox"/> SAME AS RPT <input type="checkbox"/> DTIC USERS			21. ABSTRACT SECURITY CLASSIFICATION UNCLASSIFIED		
22a. NAME OF RESPONSIBLE INDIVIDUAL Dr. Won B. Roh			22b. TELEPHONE (Include Area Code) (513) 255-2012	22c. OFFICE SYMBOL AFIT/ENP	